A combined molecular dynamics simulation, experimental and coupling model study of the ion dynamics in glassy ionic conductors

2003 J. Phys.: Condens. Matter 15 S1607

(http://iopscience.iop.org/0953-8984/15/16/310)

INSTITUTE OF PHYSICS PUBLISHING JOURNAL OF PHYSICS: CONDENSED MATTER

J. Phys.: Condens. Matter **15** (2003) S1607–S1632 PII: S0953-8984(03)60762-9

A combined molecular dynamics simulation, experimental and coupling model study of the ion dynamics in glassy ionic conductors

K L Ngai[1,5], J Habasaki[2], Y Hiwatari[3] and C León[4]

[1] Naval Research Laboratory, Washington, DC 20375-5320, USA
[2] Tokyo Institute of Technology, Nagatsuta 4259, Yokohama 226-8502, Japan
[3] Kanazawa University, Kakuma, Kanazawa 920-1192, Japan
[4] GFMC, Departamento Física Aplicada III, Facultad de Ciencias Físicas, Universidad Complutense de Madrid, Avenida Complutense s/n, 28040 Madrid, Spain

E-mail: ngai@estd.nrl.navy.mil

Received 12 March 2003
Published 14 April 2003
Online at stacks.iop.org/JPhysCM/15/S1607

Abstract

Dielectric relaxation measurements of the ion dynamics in glassy, molten and crystalline ionic conductors show general properties independent of chemical composition and structure. These include the appearance of a near-constant loss at high frequencies/low temperatures and the transition to a many-particle ion-hopping regime at lower frequencies. We use a combination of molecular dynamics simulation, experimental data analysis and the coupling model to characterize the ion dynamics in the near-constant-loss regime, the transition zone, and the many-particle ion-hopping regime. An improved understanding is gained of the origin of the near-constant loss and the evolution of the ion dynamics, from short times when the ions are caged, to long times when they are no longer caged but participate in the many-particle dynamics, giving rise finally to dc conductivity. Reasons are given to refute criticism of use of the electric modulus to represent and interpret experimental data.

1. Introduction

In crystalline, molten and glassy ionic conductors a near-constant dielectric loss (NCL),

$$\varepsilon''_{\mathrm{NCL}}(\omega) \approx A\omega^{-\alpha}, \tag{1}$$

where α is nearly zero, invariably appears in the frequency spectrum at sufficiently high frequencies and low temperatures [1–21]. The intensity of the NCL, A, is independent of ω and has a weak temperature dependence that is often well described by either T^{λ} or $\exp(T/T_0)$,

[5] Author to whom any correspondence should be addressed.

where λ is a positive power not much larger than unity and T_0 is a temperature usually larger than T. The NCL corresponds to an almost linear frequency dependent real part of the complex conductivity,

$$\sigma'_{\rm NCL}(\omega) = \omega\varepsilon''(\omega) \approx A\omega^{1-\alpha}. \tag{2}$$

This NCL contribution can no longer be seen at lower frequencies and/or higher temperatures, gradually giving way to the final appearance of the ion-hopping ac conductivity, $\sigma'_{hop}(\omega)$. The latter is assumed by some workers to be represented by the Jonscher expression [22],

$$\sigma^*_J(\omega) \equiv \sigma'(\omega) + {\rm j}\sigma''(\omega) = \sigma_0[(1 + ({\rm j}\omega/\omega_p)^{n_J}], \tag{3}$$

where n_J is a fractional exponent, σ_0 is the dc conductivity and ω_p is a characteristic relaxation frequency. Alternatively [23], the ion-hopping ac conductivity can be well described by using the one-sided Fourier transform,

$$M^*(\omega) = M' + {\rm i}M'' = M_\infty\left[1 - \int_0^\infty {\rm d}t\,\exp(-{\rm i}\omega t)(-{\rm d}\Phi/{\rm d}t)\right], \tag{4}$$

of the Kohlrausch stretched exponential function,

$$\Phi(t) = \exp[-(t/\tau_K)^{1-n}]. \tag{5}$$

By combining these two equations, the ion-hopping contribution to the complex electric modulus, $M^*_n(\omega)$, is obtained and the corresponding dielectric loss, $\varepsilon''_n(\omega)$, and conductivity, $\sigma'_n(\omega)$, are given by the relations $\varepsilon''_n(\omega) = {\rm Im}[1/M^*_n(\omega)]$ and $\sigma'_n(\omega) = {\rm Re}[{\rm i}\omega\varepsilon_0/M^*_n(\omega)]$ respectively. Similar to Jonscher's expression, $\sigma'_n(\omega)$ takes the dc conductivity σ_0 at low frequencies but increases as a power law $(\omega\tau_K)^n$ at high frequencies, instead of as the Jonscher expression $(\omega/\omega_p)^{n_J}$. Both σ_0 and the electrical conductivity relaxation time τ_K of equation (5) have the same temperature dependence. Evidence in support of ion–ion correlations being responsible for the stretched exponential time dependence of the electrical relaxation, and therefore a many-particle ion-hopping transport contribution to $\sigma'_n(\omega)$, comes from the concentration dependence of the exponent, $1 - n$, [17, 18] and molecular dynamics (MD) simulation results [24].

The properties of the NCL differ [16] in many respects from $\sigma'_n(\omega)$. For example, while $\sigma'_{\rm NCL}(\omega)$ has a weak temperature dependence, either $\sigma^*_J(\omega)$ or $\sigma'_n(\omega)$ has a strong thermally activated temperature dependence. From the properties of the NCL, it was concluded that it nevertheless comes from motion of the ions [16]. The evidence includes the observed approximately linear increase of the NCL with concentration of mobile ions [8, 16], the very different effect seen by mixing different alkalis [16] and the existence of the NCL in crystalline ionic conductors containing a high concentration of mobile ions [25–27]. The objective of this work is to use MD simulations in conjunction with experimental data to characterize the ion dynamics in the NCL regime, the many-particle ion-hopping regime and the transition zone in between the two. From the data we determine one crossover frequency, $\omega_{x1} \equiv 2\pi\nu_{x1} \equiv 1/t_{x1}$, for which the NCL exists above, and another, $\omega_{x2} \equiv 2\pi\nu_{x2} \equiv 1/t_{x2}$, for which $\sigma'_n(\omega)$ behaviour is found below. Then, the coupling model (CM) is employed to provide the independent ion-hopping relaxation time, τ_0, or frequency $\omega_0 \equiv 2\pi\nu_0 \equiv 1/\tau_0$, which turns out to lie in between ω_{x1} and ω_{x2} i.e. the transition zone between the NCL and $\sigma'_n(\omega)$. This finding leads to an interpretation of the origin of the NCL and the evolution of the complex ion dynamics with time, from short times when the ions are caged to long times when there is many-particle long-ranged ionic motion (as described by $\sigma'_n(\omega)$). The weak temperature dependence of the NCL is also a consequence of the model. As a disclaimer, our analysis does not give a complete explanation of the NCL including its observed frequency dependence. The main result is just

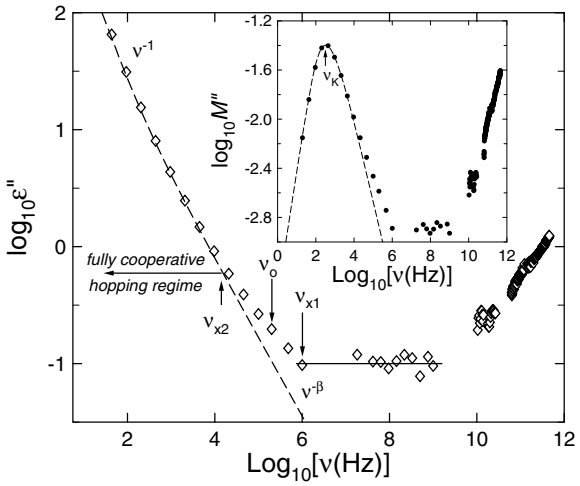

Figure 1. Dielectric loss as a function of frequency for CKN at 342 K showing the existence of the NCL (horizontal full curve) over three decades of frequency. The dashed curve is the many-particle ion conductivity relaxation calculated from the Kohlrausch fit to the electric loss modulus, M'', data shown in the inset as the dashed line with $\beta = 0.66$. The deviation of the data from the Kohlrausch fit at higher frequencies is marked by one crossover frequency, ν_{x2}. The deviation of the data from the NCL at lower frequencies is marked by the other crossover frequency, ν_{x1}. The location of the independent relaxation frequency $\nu_0 \equiv 1/2\pi\tau_0$ is also indicated where τ_0 is the independent ion-hopping relaxation time calculated from the CM. The data are from [39] and [40].

$t_{x1} \ll \tau_0 \ll t_{x2} \ll \tau_K$. The first inequality merely suggests an interpretation of the NCL which is supported by the MD simulations.

The paper is organized as follows. In section 2, we use several examples of the isothermal $\sigma'(\omega)$ data for glassy and molten ionic conductors to characterize the crossover frequencies ν_{x1} and ν_{x2}. In section 3 the CM is employed to calculate the independent ion-hopping relaxation frequency, ν_0, [28–32] and it is compared with ν_{x1} and ν_{x2} in section 4. From these findings, and as described in section 5, an interpretation can be given of the NCL and the transition to a many-particle ion-hopping regime. One consequence of our interpretation of the NCL is a weak temperature dependence which is derived in section 6. An MD simulation of the metasilicate glass Li_2SiO_3 is presented in section 7 and the results, including the mean square displacement (MSD) of the Li^+ ions, the self-part of the van Hove correlation function for the Li^+ ions and the non-Gaussian parameter, are found to support our interpretation of the ion dynamics given in previous sections. In section 8, reasons are given to refute criticism of use of the electric modulus to represent and interpret experimental data. Finally, the paper ends with a summary and conclusion.

2. The crossover frequencies ν_{x1} and ν_{x2} derived from several example experimental data sets

2.1. Molten $0.4Ca(NO_3)_2$–$0.6KNO_3$ *(CKN)*

Lunkenheimer *et al* [33, 34] made electrical relaxation measurements on molten CKN over an unusually broad frequency and temperature range. In figure 1, we show first their ε'' data at 342 K as a function of frequency, ν, which is related to the angular frequency ω by $\omega = 2\pi\nu$. The data shown by diamonds in this figure indicate the existence of an NCL that extends

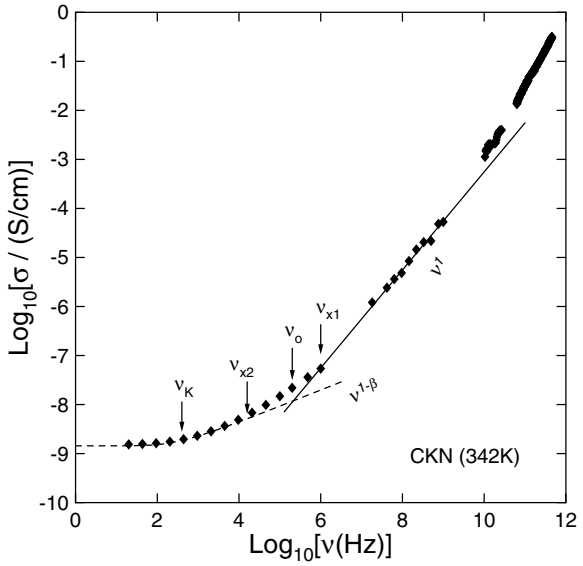

Figure 2. Re-plot of the CKN data of figure 1 as $\log_{10}\sigma'(\nu)$ versus log(frequency/Hz) to show the near-linear frequency dependence of the NCL in figure 1. The dashed curve, representing the many-particle ion conductivity relaxation, includes the dc conductivity and the high-frequency power law $\nu^{1-\beta}$ (or ν^n) dependence corresponding to a Kohlrausch fit to the electric modulus as shown by the dashed line in the inset of figure 1 with $\beta = 0.66$ (or $n = 0.34$).

over about three decades of frequency and there is a crossover to a power law dependence $\varepsilon''(\nu) \propto \nu^{-\beta}$ at lower frequencies (with $\beta = 1 - n$) and eventually to a $\varepsilon''(\nu) \propto \nu^{-1}$ dependence at even lower frequencies in the dc conductivity regime. The inset of figure 1 shows the *same* data but as $M''(\nu)$. The dashed curve is the fit by equations (4) and (5) to the data with $\beta \equiv (1 - n) = 0.66$ and $\tau_K = 6.6 \times 10^{-4}$ s. The data in the M'' representation also show the crossover from NCL to a power law $M'' \propto \nu^{-\beta}$ dependence. Although this crossover is broad for both ε'' and M'', it is observed that the end of the NCL regime occurs quite abruptly as found previously for $Li_{0.18}La_{0.6}1TiO_3$ (LLTO) [20]. It is worthwhile pointing out that the dashed line in the main part of figure 1 having a ν^{-1} dependence at low frequencies and a $\nu^{-\beta}$ dependence at higher frequencies is actually $\varepsilon_n''(\nu)$ calculated from a fit to the electric modulus by using the identity $\varepsilon_n''(\nu) = \mathrm{Im}\{1/M_n^*\}$, the loss from the many-particle hopping of ions.

Some readers may be more familiar with the NCL having a near ν^1 dependence in the $\sigma'(\nu)$ representation of the data as shown in figure 2. In this figure the dashed curve that tends to the dc conductivity at low frequencies and the power law $\nu^{(1-\beta)}$ at high frequencies is $\sigma_\beta'(\nu)$ as calculated from the identity $\sigma_\beta'(\nu) \equiv \omega\varepsilon_\beta''(\nu)$ and again it arises from many-particle ion hopping. The NCL terminates at lower frequencies quite distinctly at ν_{x1} as also seen by inspection of figure 1 through the rapid rise of $\varepsilon''(\nu)$ from the flat loss at frequencies below ν_{x1}. On further lowering the frequency, ε'' and M'' assume the $\nu^{-\beta}$ dependence and $\sigma'(\nu)$ assumes the $\nu^{1-\beta}$ dependence of the many-particle ion-hopping regime starting at ν_{x2}. Thus the crossover of the $\varepsilon''(\nu)$ data from NCL to $\varepsilon_\beta''(\nu)$ (or the $\sigma(\nu)$ data from NCL to $\sigma_\beta'(\nu)$) is not sharp, occurring over a frequency range, $\nu_{x1} > \nu > \nu_{x2}$. The values of ν_{x1} and ν_{x2} depend on the criterion used to describe when crossover has occurred. We use a 5% deviation as this criterion whenever there are enough data points for this purpose.

Having used an example experimental data set to explain the procedure used for determining the crossover frequencies, we analyse in exactly the same manner the isothermal

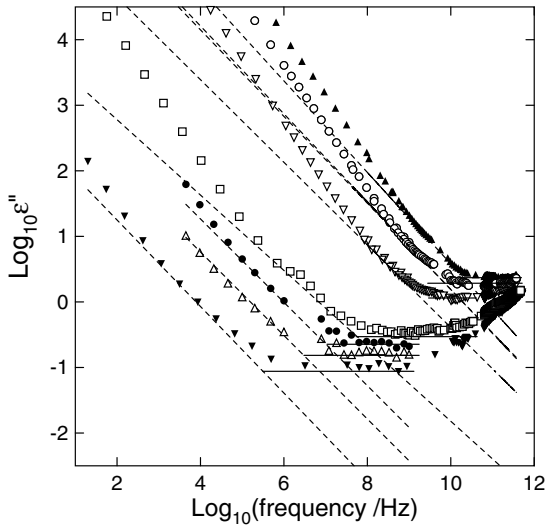

Figure 3. Symbols represent the dielectric loss data of Lunkenheimer *et al* [33, 34] for CKN at 342.0, 350.3, 356.4, 362.0, 393.0, 417.0 and 440.0 K (from bottom to top). The dashed lines represent the loss due to many-particle ion hopping as calculated from Kohlrausch fits to the electric modulus data and converted to a dielectric loss function of frequency. The horizontal full curves show the NCL. The crossover frequencies ν_{x1} and ν_{x2} (not shown) are determined from these data in the same manner as explained for figure 1.

$\varepsilon''(\nu)$ data of Lunkenheimer *et al* [33, 34] for more temperatures shown in figure 3. For all temperatures, the dashed line shows the $\nu^{-\beta}$ dependence of $\varepsilon''_\beta(\nu)$ calculated from M''_β (the fit to $M''(\nu)$ data by equations (4) and (5)) and extrapolated to higher frequencies. The relaxation times $\tau_K(T)$ obtained from the fits are converted to frequencies, $\nu_K \equiv 1/(2\pi\tau_K(T))$, which are shown in figure 4 as filled squares. In the same figure the crossover frequencies $\nu_{x1} \equiv 1/(2\pi t_{x1})$ and $\nu_{x2} \equiv 1/(2\pi t_{x2})$ determined from the data in figure 3 and at other temperatures are also shown (open diamonds for ν_{x1} and filled diamonds for ν_{x2}). By definition, t_{x1} and t_{x2} are naturally the crossover times. The crossover region is narrower at higher temperatures and, although broader at lower temperatures, the region is only about two and a half decades wide at 324 K, the lowest measurement temperature below the glass transition temperature T_g. The independent ion-hopping frequency, $\nu_0 \equiv 1/(2\pi\tau_0)$, located between ν_{x1} and ν_{x2} in figures 1–4, will be discussed later.

2.2. *Glassy* $0.80LiF$–$0.20Al(PO_3)_3$

Electrical relaxation data at 293 K for the glassy ionic conductor 0.80LiF–0.20Al$(PO_3)_3$ were obtained by Kulkarni *et al* [35] over an unusually broad frequency range. In figure 5, we show their data for σ' as a function of frequency ν. The existence of the NCL is exemplified by a near-linear frequency dependence of the σ' data over about two decades, which starts to terminate at ν_{x1}. The inset of figure 5 shows the *same* data in terms of $M''(\nu)$ only up to 10^6 Hz to isolate the contribution from many-particle ion hopping. The line is the Kohlrausch fit by equations (4) and (5) to the $M''(\nu)$ data with $\beta \equiv (1-n) = 0.56$ and $\tau_K = 8.7 \times 10^{-5}$ s. At high frequencies the Kohlrausch fit to M'' assumes a $\nu^{-\beta}$ dependence and the corresponding $\sigma'_\beta(\nu)$ assumes a $\nu^{1-\beta}$ dependence, which is shown by the straight line with slope 0.44 in figure 5. The $\sigma'(\nu)$ data conform to a $\nu^{1-\beta}$ dependence for $\sigma'_\beta(\nu)$ at frequencies below ν_{x2}.

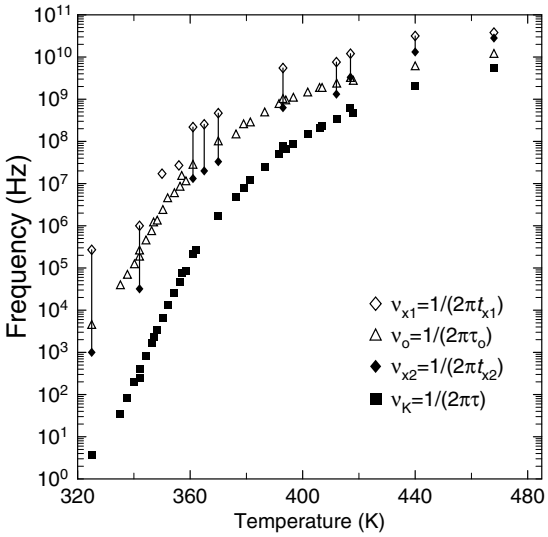

Figure 4. Solid squares are the Kohlrausch conductivity relaxation frequency $\nu_K \equiv 1/(2\pi\tau_K)$, where τ_K is obtained from fits to the data for CKN in the electric modulus representation. Open triangles represent $\nu_0 \equiv 1/(2\pi\tau_0)$, where τ_0 is the independent ion-hopping relaxation time of the CM calculated using $t_c = 2$ ps and the fitted τ_K and n values. The open and closed diamonds are the crossover frequencies ν_{x1} and ν_{x2} obtained in the same manner as described for figures 1 and 2.

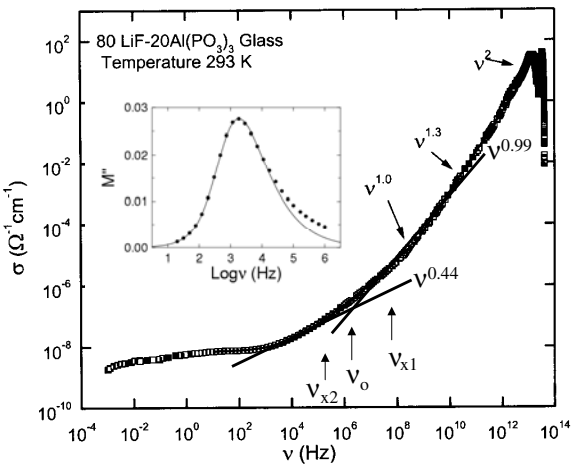

Figure 5. $\log_{10}\sigma'(\nu)$ versus log(frequency/Hz) plot of data at 293 K for 0.80LiF–0.20Al$(PO_3)_3$ obtained by Kulkarni *et al* [35] to show the near-linear frequency dependence of the NCL by the straight line with slope equal to 0.99. The straight line with slope 0.44 is the high-frequency dependence of $\log_{10}\sigma'(\nu)$ corresponding to the Kohlrausch fit to the electric modulus data (shown in the inset) with $n = 0.44$. The crossover frequencies ν_{x1} and ν_{x2} as well as the independent ion-hopping frequency ν_0 are determined from the data in the same manner as explained for figure 1.

Thus, just like CKN, the $\sigma'(\nu)$ data for 0.80LiF–0.20Al$(PO_3)_3$ show a crossover from NCL to $\sigma'_\beta(\nu)$ over a frequency range $\nu_{x1} > \nu > \nu_{x2}$.

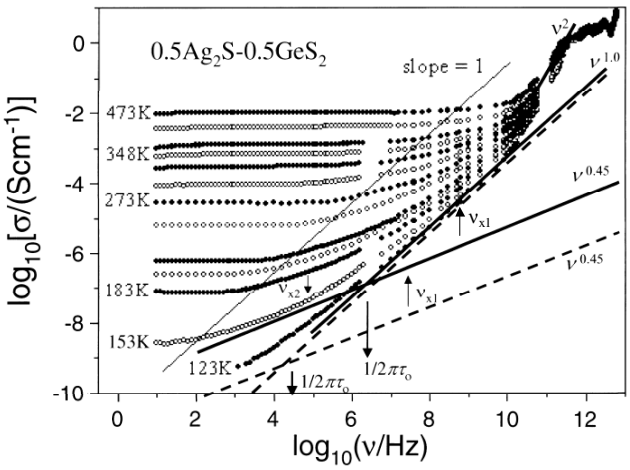

Figure 6. As figure 5 but for glassy $0.5Ag_2S$–$0.5GeS_2$ (data from the work of Berlin *et al* [13, 36]). The solid and dashed straight lines with unit slope indicate the NCL for $T = 153$ and 123 K respectively. The straight line with slope 0.45 is the high-frequency dependence of $\log_{10}\sigma'(\nu)$ corresponding to the Kohlrausch fit to the electric modulus data (not shown) with $n = 0.45$. The crossover frequencies ν_{x1} and ν_{x2} as well as the independent ion-hopping frequency $\nu_0 \equiv 1/(2\pi\tau_0)$ are determined from the data at 153 K in the same manner as explained for figure 1. The arrow at the very bottom indicates the location of $\nu_0 \equiv 1/(2\pi\tau_0)$ at 123 K.

2.3. *Glassy* $0.5Ag_2S$–$0.5GeS_2$

Figure 6 shows the data for glassy $0.5Ag_2S$–$0.5GeS_2$ at many temperatures taken from the work of Belin *et al* [13, 36]. Only the data at 153 and 123 K are considered here because they show clearly the existence of the NCL over extensive frequency domains as indicated by the solid (for 153 K) and dashed (for 123 K) straight lines with $\nu^{1.0}$ dependence. The weak temperature dependence of the NCL is evident from the proximity of the two lines. The two upward pointing vertical arrows labelled by ν_{x1} indicate the location of ν_{x1} for 153 K (at higher frequency) and 123 K (at lower frequency). Only ν_{x2} can be determined from the data at 153 K and is indicated by a similarly labelled arrow. The location of the independent ion-hopping frequency, $\nu_0 \equiv 1/(2\pi\tau_0)$, at 153 K is indicated by the longer downward arrow and lies in between ν_{x1} and ν_{x2}. The shorter downward arrow is $\nu_0 \equiv 1/(2\pi\tau_0)$ for 123 K.

2.4. *Glassy* $xNa_2O\cdot(1-x)[0.04B_2O_3$–$0.96SiO_2]$ *with* $x = 0.000\,44$

The Vycor glass $x\mathrm{Na_2O}\cdot(1-x)[0.04\mathrm{B_2O_3}$–$0.96\mathrm{SiO_2}]$ with $x = 0.000\,44$ contains very few $\mathrm{Na^+}$ ions [37]. Nevertheless, its conductivity relaxation data measured at 313 °C (figure 7) show the existence of the NCL at higher frequencies and the crossover to a near-exponential time dependent ion hopping with a small n value of 0.05. In figure 7, arrows indicate the locations of ν_K, ν_0 and ν_{x1} but the location of ν_{x2} is not indicated because the data do not allow us to determine it with confidence.

2.5. *Glassy* xK_2O–$(1-x)GeO_2$ *with* $x = 0.02$ *and* 0.0023

A similar situation to the Vycor glass is found for the conductivity relaxation data of Jain and Krishnaswami [18] for two $x\mathrm{K_2O}$–$(1-x)\mathrm{GeO_2}$ glasses with $x = 0.02$ and 0.0023. The many-particle ion hopping was characterized by a Kohlrausch fit to the electric modulus data

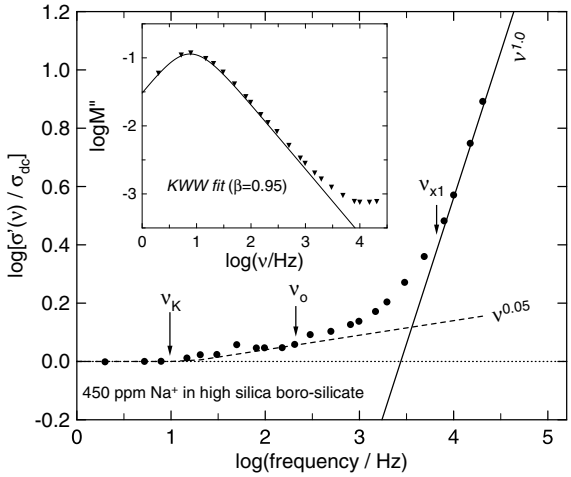

Figure 7. As figure 5 but for the Vycor glass $x\mathrm{Na_2O}\cdot(1-x)[0.04\mathrm{B_2O_3}–0.96\mathrm{SiO_2}]$ with $x = 0.000\,44$ at 313 °C (data after Simmons *et al* [37]). Here n is equal to 0.05. Arrows indicate the locations of the frequencies ν_{x1}, ν_0 and ν_K.

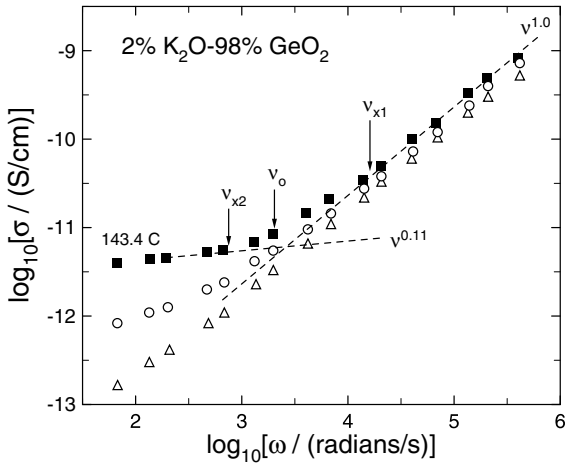

Figure 8. As figure 5 but for a $x\mathrm{K_2O}–(1-x)\mathrm{GeO_2}$ glass with $x = 0.02$ (data after Jain and Krishnaswami [18]). Here n is equal to 0.11 as obtained by Jain and Krishnaswami from a fit to the electric modulus (not shown). Arrows indicate the crossover frequencies, ν_{x1} and ν_{x2}, as well as the frequency ν_0.

with $\beta \equiv (1-n) = 0.89$ and 0.93 for $x = 0.02$ and 0.0023 respectively. In figure 8 we show only the data for $x = 0.02$ at 143.4 °C and draw two lines corresponding to the two power laws $\nu^{1.0}$ and $\nu^{0.11}$ (dashed curves). From these lines and the experimental data we determined the two crossover frequencies.

3. The independent ion-hopping relaxation time τ_0 from the CM

The CM for ionic conductors [5, 30–32] used in the past considered only the long-time regime when *all* of the mobile ions have a high probability of hopping out of their cages. All of them

are ready to hop to neighbouring sites with a relaxation rate τ_0^{-1} but a simultaneous independent hopping of each ion is made impossible by their interactions and correlations. The result is a slowed-down motion for all the ions and complex many-particle dynamics. The correlation function is changed at some time t_c, determined by the ion–ion interactions, from the linear exponential,

$$\Phi(t) = \exp(-t/\tau_0), \tag{6}$$

for independent hopping to the stretched exponential function, $\exp[-(t/\tau_K)^{1-n}]$, given by equation (5). The relation between τ_K and τ_0 is given by

$$\tau_K = [t_c^{-n}\tau_0]^{1/(1-n)} \tag{7}$$

with $t_c = 2$ ps determined previously from high-frequency measurements on ionic conductors [38–45]. Experimental evidence for the existence of such a change of dynamics in the neighbourhood of t_c is found from the high-frequency and *highest*-temperature $\sigma(\omega)$ measurements of Cramer *et al* [38, 39, 43, 44] on molten CKN, glassy 0.44LiBr–0.56 Li_2O–B_2O_3 and other glasses, after the ω^2-dependent vibrational absorption contribution is removed from the data. The temperature must be high enough that there is no intervening NCL and the many-particle ion-hopping term (having at high frequencies a ν^n dependence for the ac conductivity) crosses over directly to the independent ion-hopping term (having a frequency independent conductivity). An example can be found at the highest measurement temperature 573 K for 0.44LiBr–0.56Li_2O–B_2O_3 [38], where the spectrum shows no intervening NCL and therefore, after subtracting out the vibrational contribution, the results should arise solely from ion diffusion. The conductivity results are found to level off rather abruptly at about 10^{11} Hz (or a time of about 2 ps) to a plateau, i.e. a frequency independent value, which corresponds to the exponential correlation function given by equation (6). Thus a change from independent ion-hopping (equation (6)) to many-particle ion-hopping (equation (5)) with decreasing frequency at about 10^{11} Hz, or a time $t_c \approx$ 1–2 ps, is evident from this data. Similar changes were found for the crystalline ionic conductors Na β-alumina [40, 41, 45] and $RbAgIO_4$ [42].

Other evidence for a change of dynamics near $t_c \approx$ 1–2 ps is found from the change in the temperature dependence of the dc conductivity for many ionic conductors when it exceeds about 1 S cm^{-1} [31]. Other support comes from quasi-elastic neutron scattering (time-of-flight) experiments used to study the short-time (in the picosecond and sub-picosecond range) behaviour of the ionic diffusion coefficient as a function of temperature in the super-ionic glasses AgI–$AgPO_3$ and 0.5Ag_2S–0.5GeS_2 [46–48]. The data for 0.5Ag_2S–0.5GeS_2, the same material as discussed earlier in section 2.3, played a pivotal role in the interpretation of the data for AgI–$AgPO_3$ because the former contains no AgI and yet the results for both glasses are similar. From the quasi-elastic neutron scattering data it was found that the activation enthalpy of the short-time diffusion coefficient, E_a, is smaller than E_σ for the dc conductivity [48] and is approximately equal to $(1-n)E_\sigma$ [40, 41]. The results are shown in table 1 where $(1-n) \equiv \beta$ is the Kohlrausch exponent of the many-particle ion hopping described by equation (5) and E_σ is the activation enthalpy of the many-particle ion-hopping relaxation time τ_K in equation (5) or the dc conductivity at much lower temperatures and longer times than those explored in the quasi-elastic neutron scattering experiments. It is easy to verify from equation (7) that the product, $(1-n)E_\sigma$, is the activation enthalpy for the independent ion-hopping relaxation time τ_0. Thus, quasi-elastic neutron scattering measurements made in the picosecond and sub-picosecond range find that ions hop independently in this short-time regime, indicating that t_c is of the order 1 ps.

The independent relaxation time $\tau_0(T)$ of the CM can be calculated by equation (7) using $t_c = 2$ ps and the experimental values for τ_K and $(1-n)$, obtained from fitting $M^*(\omega)$ data by $M_n^*(\omega)$using equations (4) and (5). In the CM, $\tau_0(T)$ is interpreted as

Table 1. Activation enthalpies, E_a, for glassy $0.5AgI–0.5AgPO_3$ [46, 47] and $Ag_2S–GeS_2$ [48] obtained from the short-time ionic diffusion as studied by quasi-elastic neutron scattering. Also included are the Kohlrausch exponent, $\beta \equiv (1-n)$, and the activation enthalpy, E_σ, for conductivity relaxation observed in the same glasses [40, 41] at lower temperatures and frequencies in the many-particle ion-hopping regime. A near equality between E_a and βE_σ is found, consistent with a change to independent relaxation at times shorter than $t_c \approx 2$ ps as probed by quasi-elastic neutron scattering.

Glass	E_σ	β	βE_σ	E_a
$AgI–AgPO_3$	21 (kJ mol^{-1})	0.44	9.2 (kJ mol^{-1})	8.7 (kJ mol^{-1})
$Ag_2S–GeS_2$	0.34 eV	0.45	0.153 eV	0.15 eV

the relaxation time for an ion, vibrating in its potential well, to exit by overcoming the energy barrier E_a through thermal activation, provided it is possible to neglect the effects caused by ion–ion correlations/interactions [30–32]. If τ_K has the Arrhenius temperature dependence, $\tau_K(T) = \tau^*_\infty \exp(E^*_a/kT)$, and n is constant over a temperature region, then it follows from equation (7) that $\tau_0(T)$ should also have an Arrhenius temperature dependence, $\tau_0(T) = [t_c^n \tau_K^{1-n}] = \tau_\infty \exp(E_a/kT)$, over the same temperature range where $E_a = (1-n)E^*_a$. From the simple nature of τ_0, the reciprocal of its pre-factor, τ_∞, must be identifiable with the vibrational angular frequency of an ion inside its potential well as verified by experiment. An example indicating that τ_0 is indeed the thermally activated relaxation time for an ion to hop out of its potential well is provided by a CM analysis of the conductivity relaxation and hyper-Raman scattering data for yttria stabilized zirconia (YSZ) [30].

Most if not all of the previous applications of the CM dealt with many-particle ion hopping in the long-time regime $t > \tau_0$ when *all* ions have a high probability of executing an independent hopping motion which is, however, pre-empted by the ion–ion correlations/interactions. In this previous work, the ion dynamics in the early-time regime, $t < \tau_0$, when most of the mobile ions are still caged, was not considered. At sufficiently short times/low temperatures, few ions succeed in moving away from their original sites. Naturally, for $t \ll \tau_0$, these successful hops are executed by independent ion jumps with a rate τ_0^{-1} because the probability, given by $\exp(-t/\tau_0)$, is small such that successful hops are few and infrequent. There is, therefore, an absence of any effect from ion–ion correlations i.e. no co-operativity is involved. The number of independent hops increases with time throughout this early time regime albeit very slowly, causing a very slow decay of the cages. The near-constant loss then originates from a very slow increase of the MSD of the mobile ions or from a slow decay of the cage correlation function with time. Ultimately the NCL comes from those few and infrequent ions that have hopped out of their cages to neighbouring sites over decades of time in this short-time regime, $t < t_{x1}$. Only for times short compared with τ_0, or equivalently for frequencies high compared with $\nu_0 \equiv 1/2\pi\tau_0$, will successful hops from cages be few and infrequent. Thus the NCL exists only at times much shorter than τ_0 or frequencies much higher than ν_0 i.e. $t_{x1} \ll \tau_0$. This point will be revisited after a comparison of ν_0 with ν_{x1} and ν_{x2} for CKN has been made.

4. Relation of ν_0 with ν_{x1} and ν_{x2}

The ion conductivity relaxation data of CKN in figures 1–3 were analysed by equations (4) and (5) and the two parameters $\tau_K(T)$ and $(1 - n(T))$ determined by Lunkenheimer *et al* [33, 34]. The data covered an extended temperature range from below to above the glass transition temperature, T_g. Typical for the relaxation of glass-forming substances above T_g, the relaxation frequency $\nu_K \equiv 1/2\pi\tau_K$ is not Arrhenius and the Kohlrausch parameter

$\beta \equiv (1-n(T))$ is temperature dependent. From these parameters, the independent ion-hopping relaxation time $\tau_0(T)$ was also calculated by Lunkenheimer *et al* [33, 34] and for CKN the experimentally determined t_c value is 2 ps [38, 39]. The independent ion-hopping frequency, $\nu_0 \equiv 1/2\pi\tau_0$, is plotted against temperature in figure 4. At high temperatures where ν_{x1} and ν_{x2} are close to each other, $\nu_0(T)$ lies close to these two frequencies. At lower temperatures the crossover region, $\nu_{x1} > \nu > \nu_{x2}$, becomes broader but it is remarkable that ν_0 invariably falls inside it.

In a similar manner to that described for CKN in the preceding paragraph, we determined ν_0 for other glassy and crystalline ionic conductors, some examples of which were considered in sections 2.2–2.5. When comparing ν_0 with ν_{x1} and ν_{x2} in figures 5–8, we again find for these other ionic conductors that $\nu_{x1} > \nu_0 > \nu_{x2}$, as for the molten salt CKN. The present relation found between ν_0 and the crossover frequencies ν_{x1} and ν_{x2} for glassy and molten CKN and other glassy and crystalline ionic conductors may not be an accident because they are independently and separately determined quantities. Firstly, ν_0 is determined from the low-frequency many-particle ion-hopping dispersion corresponding to equations (4) and (5) by using the CM relation of equation (7). Secondly, ν_{x1} and ν_{x2} are determined separately from the termination of two loss mechanisms, the NCL regime and the many-particle ion-hopping regime (equations (4) and (5)), which have very different temperature dependences. We recall that the NCL has a weak temperature dependence approximately described by $\exp(T/T_0)$ [20], while the frequency dependent loss arising from ion hopping has a strong thermally activated temperature dependence.

5. Origin of the NCL and transition to a many-particle ion-hopping regime

The general properties of the transition from the NCL to a many-particle ion-hopping conductivity regime found above suggests the following origin for the NCL. At sufficiently short times, $t \ll \tau_0$, when most of the ions are still caged, the successful ion jumps out of cages are *independent* of each other and the rate is $1/\tau_0$. Hence the probability of such events, $\exp(-t/\tau_0)$, is small and at any time there are very few such hops and therefore many-particle dynamics is not involved. At times much shorter than τ_0, independent hopping of ions out of their cages is rare and the increase of the MSD, $\langle r^2 \rangle$, with time has to be very slow. Such a slow increase of $\langle r^2 \rangle$ with time is equivalent to an NCL. This result can be seen from the following approximate relation (neglecting cross-correlations and the Haven ratio which is not unity) between the MSD, $\langle r^2 \rangle$, and complex conductivity [49]:

$$\sigma^*(\omega) = -\omega^2 \frac{Nq^2}{6kT} \int_0^\infty \langle r^2(t) \rangle \mathrm{e}^{-\mathrm{i}\omega t}\, \mathrm{d}t, \tag{8}$$

where N is the density of mobile ions, q the ion charge, k the Boltzmann constant and T the temperature. For $\langle r^2 \rangle \propto t^\alpha$, equation (8) gives $\sigma'(\omega) \propto \omega^{1-\alpha}$ and $\varepsilon''(\omega) \propto \omega^{-\alpha}$ and therefore an NCL if α is small. If the MSD would increase logarithmically with time as $\langle r^2 \rangle \propto \log t$, the dielectric loss $\varepsilon''(\omega)$ would be practically flat and approximately $\sigma'(\omega) \propto \omega^{1.0}$.

Naturally the NCL can exist only in the time regime $t \ll \tau_0$ where the number of independent hops of ions from their cages over decades of time is small and the increase in this number is very slow. The NCL terminates at some time $t_{x1} \equiv 1/2\pi\nu_{x1}$, after which the independent ion hops become more significant in number and the loss can no longer be described by equation (1). There is a more rapid increase of $\langle r^2 \rangle$ with time beyond t_{x1} and the NCL, defined by the same small exponent α in equation (1) at earlier times, no longer holds. Certainly t_{x1} has to be much smaller than τ_0 (or $\nu_{x1} \gg \nu_0$) because τ_0 is the characteristic time for the ions to independently leave their cages. The number of ions hopping out of

their cages continues to increase beyond t_{x1}, and the changes in $\langle r^2 \rangle$ become more rapid, leading to an increasing deviation from the NCL. The degree of co-operativity and dynamic heterogeneity increases with time as more and more ions hop from their cages. Finally, at times t sufficiently longer than τ_0, i.e. for $t > t_{x2} > \tau_0$, *all* ions have almost a certain probability of hopping from their cages, except their mutual correlations/interactions render impossible a simultaneous independent hopping. This marks the start of the many-particle ion-hopping regime described by the Kohlrausch stretched exponential function of equation (5) and by definition $t_{x2} \equiv 1/2\pi\nu_{x2}$ is the onset time. From $t_{x2} > \tau_0$, it follows that $\nu_{x2} < \nu_0$. When the many-particle ion-hopping regime is entered, the dependences $\langle r^2 \rangle \propto t^{1-n}$, $\varepsilon''_\beta(\nu) \propto \nu^{-1+n}$ (see figure 1) and $\sigma'_\beta(\nu) \propto \nu^n$ (see figure 2) are observed. These power laws are just the shorter-time ($t \ll \tau_K$) or higher-frequency ($\nu > \nu_K$) parts of these quantities for the many-particle ion hopping described by the Kohlrausch correlation function given by equation (5), the longer-time ($t \gg \tau_K$) parts of which are $\langle r^2 \rangle \propto t$, $\varepsilon''_\beta(\nu) \propto \nu^{-1}$ and $\sigma'_\beta(\nu) = \sigma_{dc}$ (see figures 1 and 2).

From the discussion given above, we have a rationalization for the origin of the NCL and the locations of the corresponding time regime, $t < t_{x1}$, and frequency regime, $\nu > \nu_{x1}$. We have also given physical meaning to the crossover times (frequencies), t_{x1} (ν_{x1}) and t_{x2} (ν_{x2}). The qualitative theory explains the empirical results we found from the collection of data presented in this work and includes (i) the relation $t_{x1} \ll \tau_0$ ($\nu_{x1} \gg \nu_0$) and (ii) the fact that τ_0 always lies inside the crossover region, $t_{x1} < t < t_{x2}$, or ν_0 always lies in between ν_{x1} and ν_{x2}.

The CM embodied by equations (5)–(7) was designed to explain the anomalous properties of many-particle ion hopping based on independent ion hops, which has the physically transparent independent relaxation time τ_0. All previous applications of the CM were connected with a description of the many-particle ion-hopping regime at longer times ($t > t_{x2}$). Equation (7) enables the independent relaxation time τ_0 to be calculated from the low-frequency ($\nu < \nu_{x2}$) many-particle ion-hopping experimental data. Thus the empirical results found in this work and summarized in the previous paragraphs show that the CM also has an impact on the NCL and the broad crossover from the NCL to the many-particle ion-hopping regime. The impact is the ability of τ_0 to set a limit on the time, t_{x1}, when the NCL is terminated (i.e. $t_{x1} \ll \tau_0$), to locate the timescale of the transition zone and the onset time, t_{x2}, for the full many-particle ion hopping described by the Kohlrausch function of equation (5). From τ_0, one can determine the conductivity relaxation time τ_K by equation (7) and, via equations (4) and (5), the measured dispersion and the dc conductivity. The existence of τ_0 in many ionic conductors has direct support from dc conductivity [31], high-frequency and high-temperature conductivity relaxation [38, 39, 42–45] and high-temperature neutron scattering [41, 42, 46–48] measurements.

6. Temperature dependence of the NCL

We have proposed that the NCL exists in the short-time (high-frequency) regime, $t_{on} < t < t_{x1}$ ($\nu_{on} > \nu > \nu_{x1}$), where there are few thermally activated independent jumps of ions from their cages because $t_{x1} \ll \tau_0$. Here t_{on} (ν_{on}) is the onset time (frequency) of the NCL. From experimental data that show the NCL extending to very high frequencies, t_{on} is found to be of the order of 10^{-11}–10^{-12} s. The value of t_{x1} depends on the choice of the exponent $\alpha \approx 0$ used to define the NCL and is the time beyond which the experimental data, $\sigma'(\omega)$, departs from the $A\omega^{1-\alpha}$ dependence. However, whatever the choice of $\alpha \approx 0$, t_{x1} has to be much less than τ_0 in order to satisfy the condition for generation of the NCL that there are few independent ion jumps from their cages throughout the period $t_{on} < t < t_{x1}$. Therefore $\exp(-t_{x1}/\tau_0)$ is

still close to unity and its value is determined by the choice of the exponent α of the NCL. The value of $\exp(-t_{x1}/\tau_0)$ is fixed for all temperatures by using the convention that the NCL terminates at t_{x1}. Hence t_{x1} has the same thermally activated temperature dependence as $\tau_0 = \tau_\infty \exp(E_a/kT)$ and is written explicitly as $t_{x1}(T) = t_\infty \exp(E_a/kT)$. The activation energy E_a of τ_0 is related to the observed activation energy E_a^* of τ_K by $E_a = (1-n)E_a^*$. We consider here glassy ionic conductors having an Arrhenius temperature dependence for τ_0. For molten ionic conductors like CKN, τ_0 is non-Arrhenius and likewise $t_{x1}(T)$ as shown in figure 4.

From the very definition of t_{x1} adopted to define the termination of the NCL, the MSD $\langle r^2\rangle_{\rm NCL}$ corresponding to the NCL has to increase by the *same* small amount in the period $t_{on} < t < t_{x1}(T)$ at *all* temperatures. In other words, first we assume that the difference, $\langle r^2(t_{x1})\rangle - \langle r^2(t_{on})\rangle$, is a temperature independent constant. Second, we assume that the ratio $t_{x1}(T)/\tau_0(T)$ is also temperature independent, an assumption which is justifiable for *glassy* and *crystalline* materials with an Arrhenius temperature dependent $\tau_0(T)$ like that shown in figures 5–8, but which is not justifiable for molten ionic conductors at temperatures above T_g as in figure 4 for CKN. Third, we assume that $\langle r^2\rangle \propto t^\alpha$, with α small such that equation (8) gives the NCL with $\sigma'(\omega) \propto \omega^{1-\alpha}$ and $\varepsilon''(\omega) \propto \omega^{-\alpha}$. The third assumption is not essential to obtain the temperature dependence of the NCL in the next paragraph, but is included for completeness because it leads us to the particular frequency dependence of the NCL, $\varepsilon''(\omega) \propto \omega^{-\alpha}$ with α small. Note that the time dependence, $\langle r^2\rangle \propto t^\alpha$, in the third assumption is not explained but is merely rationalized in this work from the empirical fact that $\exp(-t_{x1}/\tau_0)$ is close to unity.

From the first assumption, the *same* increase of $\langle r^2\rangle_{\rm NCL}$ is spread over a number of decades of time given by $[\log_e(t_{x1}) - \log_e(t_{on})]/2.303$ which is independent of temperature. Therefore, the MSD is inversely proportional to $\log_e(t_{x1}/t_{on})$. From the second assumption, we have the Arrhenius temperature dependence $t_{x1}(T) = t_\infty \exp(E_a/kT)$ for t_{x1}. From these and the relation between conductivity and MSD (equation (8)), we deduce the intensity of the NCL, and the third assumption ensures the frequency dependence is that of the NCL. The intensity of the NCL in terms of the constant A in equations (1) and (2) is given by the proportionality relation,

$$A \propto \frac{1}{E_a}[1 - (kT/E_a)\log_e(t_{on}/t_\infty)]^{-1}. \tag{9}$$

This expression is well approximated by

$$A \propto \exp(T/T_0), \tag{10}$$

where $T \ll T_0$ and

$$T_0 \approx E_a/k\log_e(t_{on}/t_\infty). \tag{11}$$

T_0 is positive because $\log_e(t_{on}/t_\infty)$ is positive from the fact that $t_{x1} < \tau_0$, and t_∞ is even shorter than the pre-factor of τ_0, τ_∞, which is the reciprocal of a vibrational attempt frequency. In the above, we have taken into account the contribution of $\langle r^2\rangle_{\rm NCL}$ to the measured $\langle r^2\rangle$ but not the contribution from the vibrational dynamics, which has its own temperature dependence similar to that of the vibrational Debye–Waller factor. Inclusion of the latter will modify somewhat the temperature dependence of the NCL given by equation (9).

Thus the weak temperature dependence of the NCL is captured by our interpretation of its origin. Since the result given by equations (9) and (10) is obtained from a qualitative theory, we do not expect that it will accurately describe the temperature dependence of the NCL. In particular, over an extended temperature range another source of contribution to the NCL may come into play at very low temperatures and high frequencies, such as transitions between

asymmetric double-well potentials (ADWPs) [9, 50]. Of course, the ADWPs constitute a different source of the NCL than the slow cage decay process discussed herein.

We note from equation (9) that, at constant temperature, A should decrease with increasing E_a, should other factors like the ion concentration that determine the absolute value of A be the same for all ionic conductors. If this condition holds for many ionic conductors, then an approximate anti-correlation between A and E_a may exist at constant T. This is an important prediction that can be tested by experiment. Previously, Rivera *et al* [21] measured the intensity of the NCL, A, for alkali triborate glasses, M_2O–$3B_2O_3$, with M = Li, Na, K and Rb. They observed that A has an $m^{-1/3}$ dependence on the alkali mass, m, and this dependence led them to speculate that vibrational relaxation is at the origin of the NCL. The new interpretation of the NCL given in this work was not then available but now replaces the earlier speculation: its prediction that $A \propto 1/E_a$ replaces the less general observation that $A \propto m^{-1/3}$. The former can be rigorously tested by using the alkali triborate glass data of Rivera *et al* [21] and calculating E_a from the experimentally determined activation energy E_a^* for τ_K by using the relation $E_a = (1-n)E_a^*$ with $(1-n)$ taken from a fit to the terminal zone by equation (5). The results for E_a, details of which will be published elsewhere, show that it is inversely proportional to A for the family of alkali triborate glasses investigated by Rivera *et al* [21].

7. Support from molecular dynamics simulations of Li_2SiO_3

MD simulations for lithium metasilicate, Li_2SiO_3, were performed in the same way as in previous studies [51–53]. Contained in the unit cell were 144 Li, 72 Si and 216 O and the volume was fixed at that derived by an NPT (constant-number, pressure and temperature) ensemble simulation. Pair potential functions of the Gilbert–Ida type [54] and r^{-6} terms were used and the parameters for the potentials were derived on the basis of *ab initio* molecular orbital calculations [55]. The glass transition temperature determined from the T–V relation was found to be approximately 830 K and the runs at temperatures of 700, 800, 1000 and 1200 K were analysed. In the present work, we have acquired additional MD data for glassy Li_2SiO_3 glass at the low temperature of 700 K with improved statistics to show the existence of the NCL, its relation to cage decay and its gradual transition (or broad crossover) at longer times to the many-particle ion-hopping regime. The self-part of the van Hove self-correlation function, $G_s(r, t)$, for the Li^+ ions and the non-Gaussian parameter, $\alpha_2(t)$, were calculated to elucidate the ion dynamics in the NCL regime, the transition zone and the many-particle ion-hopping regime.

7.1. The mean square displacement (MSD)

The MSD, $\langle r^2 \rangle$, for Li^+ ions at 700 K is shown in figure 9 from 0.01 ps to a few thousand picoseconds. At very short times we see ballistic motion for which $\langle r^2 \rangle \propto t^2$ and at longer times a combination of the vibrational and relaxation contributions as discussed in previous work [51–53]. The vibrational contribution to the MSD becomes constant after about 1 ps. The MSD can be divided into four time regimes.

(I) An early-time regime between approximately 0.3 and 2 ps when the MSD increases very slowly like t^α with $\alpha \approx 0.1$ and can be identified with the NCL.
(II) An intermediate-time regime, $2 < t < 20$ ps, when the MSD rises increasingly more rapidly than the t^α dependence of regime I. The transition from regime I to II is used to define a crossover time that we call t_{x1} which is about 2 ps at 700 K. Thus regime I is defined by 0.3 ps $< t < t_{x1}$.

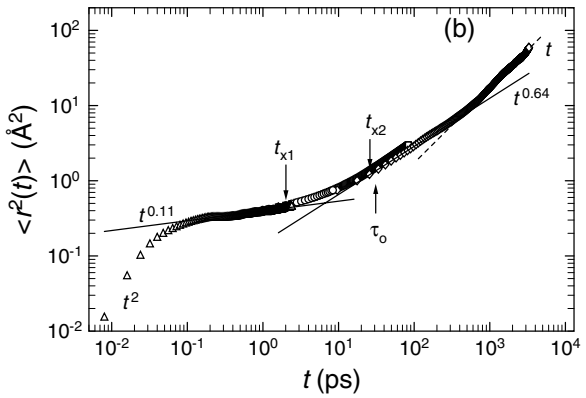

Figure 9. MSDs of Li^+ ions in Li_2SiO_3 at 700 K. t_{x1} and t_{x2} are crossover times that separate out the three time regimes explained in the text. τ_0 is the independent free jump relaxation time of a Li^+ ion calculated from equation (7) of the CM.

(III) After 26 ps and up to about 400 ps, the MSD has a time dependence described by t^β with $\beta \approx 0.64$. This time regime III corresponds to the $\omega^{1-\beta}$ power law ac conductivity for many-particle ion-hopping predicted by either the Jonscher expression (equation (1)) or the Kohlrausch expression (equation (5)) with β identified with $(1 - n)$. The time at which regime III starts defines t_{x2}, which is equal to about 26 ps at 700 K. Thus regime II is defined by $t_{x1} < t < t_{x2}$.

(IV) For times longer than about 600 ps, the MSD becomes proportional to t. At the starting time of this regime IV, the root MSD, $\sqrt{\langle r^2 \rangle}$, is about 3 Å which is the average Li^+–Li^+ ion site separation distance. By the start of this time regime, the many-particle ion-hopping process has established a steady state and the ion transport is described by the frequency-independent dc conductivity. The onset time of this regime, t_D (about 600 ps at 700 K), is not exactly the same as the τ_K of equation (5) but is of the same order of magnitude. Thus regime III is approximately defined by $t_{x2} < t < \tau_K$ and regime IV corresponds to $t > \tau_K$.

It is interesting to point out that the same properties for $\langle r^2 \rangle$ are seen from the experiments of Weeks and Weitz [56] for colloidal super-cooled liquids with a volume fraction ϕ equal to 0.52 or 0.56.

7.2. The self-part of the van Hove correlation function for Li^+ ions

The self-part of the van Hove correlation function for the Li^+ ions is defined by

$$G_s(r, t) = (1/N) \sum_{i=1}^{N} \langle \delta(r_i(t) - r_i(0) - r) \rangle, \tag{12}$$

where r is the distance travelled by a Li^+ ion in time t. The number of ions remaining in the original sites can be calculated from

$$N(t) \equiv \int_0^{r_c} 4\pi r^2 G_s(r, t)\, \mathrm{d}r, \tag{13}$$

where the first peak cut-off, r_c, is chosen to be 1.7 Å based on the behaviour of $G_s(r, t)$ at long times. This value is slightly larger than half of the distance between the Li^+ ions, $g^{\max}_{\mathrm{Li-Li}}(r)$,

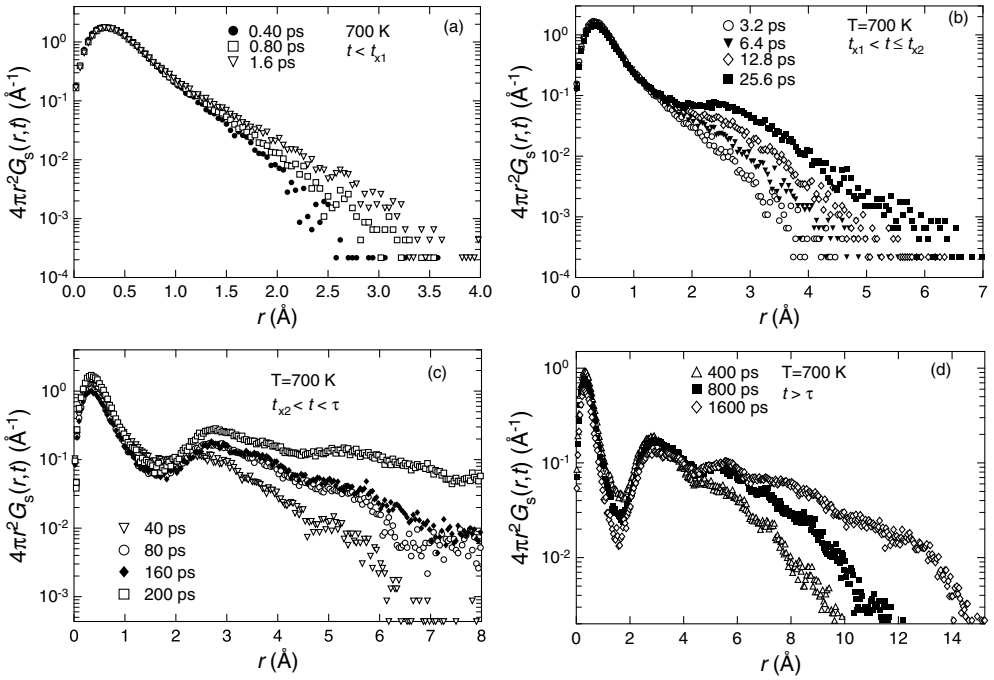

Figure 10. $4\pi r^2 G_s(r, t)$ as a function of r at different times where $G_s(r, t)$ is the self-part of the van Hove correlation function for Li^+ ions in Li_2SiO_3 at 700 K. (a) 0.40, 0.8 and 1.6 ps ($t < t_{x1}$); (b) 3.2, 6.4, 12.8 and 25.6 ps ($t_{x1} < t < t_{x2}$); (c) 40, 80, 160 and 200 ps ($t_{x2} < t < \tau_K$) where $\tau_K \approx 229$ ps is calculated (see the text); (d) 400, 800 and 1600 ps ($t > \tau_K$).

used in the previous study [51], since the difference in the viewpoints of $g_{\mathrm{Li-Li}}(r)$ and $G_s(r, t)$ is taken into account. Figures 10(a)–(d) show the evolution of $4\pi r^2 G_s(r, t)$ with time. Again we separate the time evolution into several regimes.

(I′) The times in figure 10(a) from 0.4 to 1.6 ps are within regime I in which the MSD increases very slowly like t^{α} with $\alpha \approx 0.1$ and corresponds to the NCL in the dielectric response of the glassy ionic conductor. There is only a slight increase of $4\pi r^2 G_s(r, t)$ near 3 Å with a concomitant small decrease of the first peak area. Using either one of these quantities as an indicator of the extent of cage decay, we are led to conclude that this decay is indeed very slow. A broadening of the first peak of $G_s(r, t)$ is also observed for this time region. Pre-jump motion and time dependent changes in the spatial relation of the mobile ions with the matrix atoms can be considered as the origin of this broadening. Both are related to the jump motion of the Li^+ ions and changes of the cage in a wider sense. The contribution of this broadening to the MSD is non-negligible, although in this work our attention is focused on cage decay as measured by the area under the first peak of $G_s(r, t)$.

(II′) The times in figure 10(b) from 3.2 to 25.6 ps are nearly within regime II in which the MSD increases more rapidly than in regime I but has yet to assume the constant fractional power law t^{1-n} with $(1 - n) \approx 0.7$. A shoulder located at about 3 Å appears and grows in intensity with time, indicating a more rapid cage decay than in regime I.

(III′) The times in figure 10(c) from 40 to 160 ps are within regime III in which the MSD attained the power law dependence t^{1-n} with $(1 - n) \approx 0.64$. A second peak at about 3 Å and a broad tail at longer distances appear and grow in intensity. The development of the second peak indicates that the number of ions that have left their original sites has

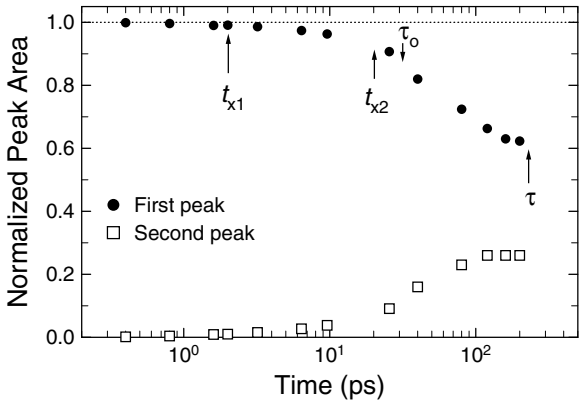

Figure 11. Time dependent normalized areas of the first peak, $A_1(t)$, and the second peak, $A_2(t)$, of the self-part of the van Hove correlation function for Li^+ ions in Li_2SiO_3 at 700 K. Vertical arrows indicate the positions of t_{x1}, t_{x2}, τ_0 and τ_K.

become significant, i.e. the cages have decayed to such an extent that a large number of ions now participate in cooperative motion with one other.

(IV′) At the longer times of 400, 800 and 1600 ps shown in figure 10(d), the second peak at ∼3 Å is fully developed and higher-order peaks become evident. In this time regime $\sqrt{\langle r^2 \rangle}$ starts at about 3 Å and the MSD of the Li^+ ions attains the $t^{1.0}$ dependence shown in figure 9.

7.3. Cage decay

In the early-time regime between approximately 0.3 and 2 ps, the MSD increases very slowly like t^α with $\alpha \approx 0.1$ and can be identified with the NCL. For ions confined in permanent harmonic and even anharmonic potential wells or cages, the MSD does not have such a very slow increase over an extended period of time like that shown in figure 9, and certainly cannot explain the NCL observed over many decades of frequencies at lower temperatures in glassy and crystalline ionic conductors. However, the cages are not permanent. There is a small but nonzero probability of the Li^+ ions independently jumping out of their original sites by thermal activation and these jumps give rise to a slow decay of the cages for other ions. The slow cage decay and the concomitant slow increase of the MSD are synergistic properties. If a cage correlation function can be defined and obtained, as in the work of Weeks and Weitz [56] for colloidal particles, the origin of NCL arises naturally from the slow cage decay. The loss can be related to the imaginary part of the Fourier transform of the cage decay correlation function. In this work we obtain the time dependent decrease of the normalized area, $A_1(t)$, of the first peak of the self-part of the Li^+ ion van Hove correlation function and use it to gauge the cage decay. Figure 11 shows the time dependence of A_1 up to about 200 ps, before the cooperative ion-hopping time regime III where the MSD has a time described by t^β with $\beta \approx 0.7$. The decrease of A_1 is very slow in time regime I between 0.3 and 2 ps, where the MSD increases very slowly like t^α with $\alpha \approx 0.1$. Thus cage decay in this time regime is the origin of the NCL, here with $\varepsilon''(\omega) \propto \omega^\alpha$ and $\alpha \approx 0.1$.

We have already mentioned that, for colloidal particles, the cage correlation function defined by Weeks and Weitz decays very slowly for times shorter than about 100 s at a volume fraction equal to 0.52 or 0.56 (see figure 2(b) of [50]). Again this and the very gradual increase

of $\langle r^2(\Delta t)\rangle$ approximately as $c(\Delta t)^\alpha$ with $\alpha \approx 0.08$ are synergistic properties, analogous to the Li^+ ion behaviour in glassy Li_2SiO_3. The ultimate origin of these two synergistic properties, as well as the NCL in glassy Li_2SiO_3, is the occurrence of independent thermally activated jumps from their cages of a small percentage of Li^+ ions which increases with time and contributes to the slow cage decay. The independent jump relaxation is an important part of the CM [28–32, 40, 41, 44, 45]. Its relaxation time τ_0 is thermally activated with energy E_a that is the same as the actual energy barrier. τ_0 is related to the longer observed conductivity relaxation time τ_K of the many-particle ion-hopping regime given by equation (7), where t_c is about 1 ps for alkali oxide glasses. At 700 K, $\tau_K \approx 229$ ps from the stretched exponential relaxation time [43] of the incoherent scattering function, $F_s(k, t)$, for $k = 2\pi/3$ Å^{-1}. This k is chosen because it corresponds to $\sqrt{\langle r^2\rangle} \approx 3$ Å, the distance between Li^+ sites. When taken together with $(1 - n) \equiv \beta = 0.64$, $t_c = 1$ ps and equation (7), τ_0 can be calculated and the result is 32 ps, which is an order of magnitude longer than t_{x1} but nearly the same as t_{x2}. This comparison between τ_0 and t_{x1} (i.e. τ_0 significantly longer than t_{x1}) explains the small probability for an independent jump of an ion from its cage during time regime I and the very slow cage decay indicated by either the MSD or A_1 calculated from the van Hove correlation function (see figure 11).

In regime II, however, when $t_{x1} < t < t_{x2}$ there is a higher probability for independent jumps, particularly with increasing time towards t_{x2} because this time is slightly shorter than τ_0. Therefore cages decay more rapidly in regime II than in regime I, a property corroborated by the time dependence of A_1 (figure 11) and the MSD (figure 9). Since t is longer than τ_0 in most of regime III, $t_{x2} < t < \tau_K$, all of the Li^+ ions are capable with high probability of executing an independent jump but instead they participate in the hopping process described by a stretched exponential correlation function for $F_s(k, t)$. Thus t_{x2} marks the change from an apparent free jump to a cooperative/correlated jump process modified by jump angles. Again this description is corroborated by the even more rapid decrease of A_1 in regime III than in regime II as can be seen by inspection of figure 11 and the steeper rise of the MSD with the power law dependence t^β with $\beta \approx 0.64$ in figure 9. The same is true for colloidal supercooled liquids. In the corresponding time regime $t_{x1} < t < t_{x2}$, the cage correlation function (see figure 2(b) of [50]) decays faster than when $t < t_{x1}$. The decay is even faster when $t > t_{x2}$.

In our present as well as in previous simulations, the localized independent jumps occur at intervals longer than the relaxation time obtained from the jump rate, indicating that there are particles having a high probability of jumping back into their original sites even in the region $t < t_{x2}$ and only a net change of the number of the particles is reflected in the peak area of the van Hove correlation functions. Therefore in time regime I, where the Li^+ ions make only independent or uncorrelated jumps, the contribution to the MSD by ions that have successfully made uncorrelated jumps, $\langle r^2\rangle_u$, is proportional to t and less than $d^2(t/\tau_0)$, where d is the localized independent jump distance for a Li^+ ion and $t \ll \tau_0$. The result follows from the fact that the jumps are uncorrelated and their number is proportional to time. It is also consistent with the correlation function for independent hops given by $\exp(-t/\tau_0)$. Now the MSD is the sum of the contributions from vibrations, relaxations and independent jumps. The contribution to the MSD from Li^+ ion vibrations, $\langle r^2\rangle_{vib}$, initially increases with time and then turns over to the constant value $kT/m\omega^2$, where m is the mass and ω the frequency, if the vibration is harmonic. In NCL regime I at 700 K, $\langle r^2\rangle_u$ rises to no more than about 40% of $\langle r^2\rangle_{vib}$. Hence the temperature dependence of the MSD is determined by $\langle r^2\rangle_{vib}$ and $\langle r^2\rangle_u$ combined. The arguments given in section 6 can also be applied to $\langle r^2\rangle_u$ to show that its temperature dependence is weak. Therefore, the temperature dependence of the MSD in regime I determined by $\langle r^2\rangle_{vib}$ and $\langle r^2\rangle_u$ combined is weak, and the computer simulation

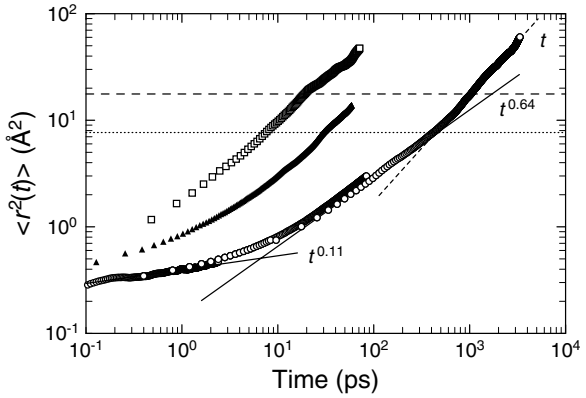

Figure 12. Time dependence of the MSD of Li^+ ions in Li_2SiO_3 at (○) 700 K, (▲) 1000 K and (□) 1200 K.

results may be used to rationalize the observed weak temperature dependence of the NCL in ionic conductors [16].

Since τ_K is thermally activated, at even lower temperatures than 700 K, τ_K (as well as τ_0) becomes much longer. At any time, the probability for independent ion jumps is further diminished. Consequently, the cage decay is even slower and t_{x1} and t_{x2} are extended to longer times. Therefore, t_{x1} and t_{x2} are temperature dependent and we can expect that this dependence is similar to that of τ_0. On the other hand, at temperatures sufficiently higher than 700 K when τ_K is not long compared with t_c, τ_0 becomes short and t_{x1} and t_{x2} are moved to shorter times. Figure 12 shows the MSDs of Li^+ ions at 1000 and 1200 K in the super-cooled liquid state. In exactly the same manner as the data at 700 K were treated, $(1 - n) \equiv \beta = 0.70$, τ_K is estimated to be 20 or 8 ps and τ_0 is calculated to be approximately 8 or 4 ps for $T = 1000$ and 1200 K respectively. The very short τ_0 of about 4 ps at 1200 K explains the earlier onset of regime III at t_{x2} estimated to be between 1 and 2 ps. Regime II is shifted to times shorter than 1 ps and regime I has disappeared into the vibrational contribution zone and no NCL can be observed. The dashed and dotted lines in figure 12 correspond to the square of the distance of the first minimum, $(4.2\ \text{Å})^2$, and to the square of the distance of the first maximum, $(2.77\ \text{Å})^2$, respectively of the Li^+–Li^+ ion pair correlation function $g_{\text{Li–Li}}(r)$ at 700 K.

7.4. The non-Gaussian parameter

The non-Gaussian parameter [57],

$$\alpha_2(t) = (3/5)\langle r^4(t)\rangle / \langle r^2(t)\rangle^2 - 1 \tag{14}$$

characterizes the deviation of $G_s(r, t)$ from Gaussian form. We have evaluated $\alpha_2(t)$ for the Li^+ ions from their time dependent displacement distribution function at 700, 800 and 1200 K. The results, plotted in figure 13 as a function of time, show that $\alpha_2(t)$ starts out from small values at short times, increases throughout regimes I and II and attains a maximum value near $t_{x2} \approx 20$ ps and $\tau_0 \approx 32$ ps. At higher temperatures, the maximum of $\alpha_2(t)$ for Li_2SiO_3 moves to shorter times and is also located near t_{x2} and τ_0 (figure 13).

The occurrence of the maximum of $\alpha_2(t)$ at a time near t_{x2} is also found in colloidal super-cooled liquids [58]. By inspection of figure 1(b) of [58], we locate the positions of the $\alpha_2(t)$ peaks at 300, 500 and 1000 s for volume fractions of 0.46, 0.52 and 0.56 respectively. These peak positions are in remarkable agreement with the t_{x2} we determined from figure 1(b)

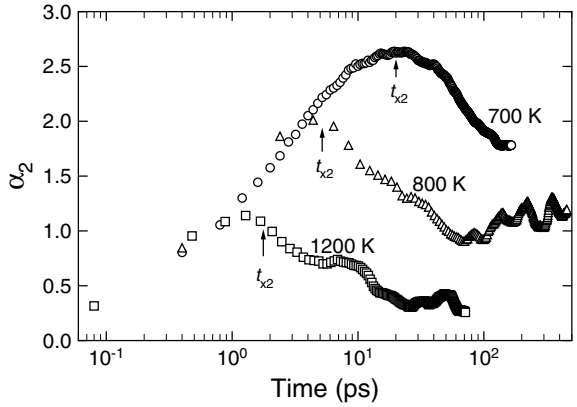

Figure 13. The non-Gaussian parameter, $\alpha_2(t)$, for Li^+ ions in Li_2SiO_3 calculated from their time dependent displacement distribution function at 700, 800 and 1200 K. At higher temperatures, the maximum of $\alpha_2(t)$ for the Li^+ ions moves to shorter times and at all temperatures the maximum is located near t_{x2}.

of [58] which are 235, 540 and 900 s for volume fractions of 0.46, 0.52 and 0.56 respectively. Thus, as in glassy Li_2SiO_3, the $\alpha_2(t)$ for colloidal super-cooled liquids peak near t_{x2}. Similar time and temperature dependences for $\alpha_2(t)$ were found from MD simulations of a super-cooled Lennard-Jones liquid [59]. These similarities of the non-Gaussian parameter, as well as properties including the time dependence of the MSD, indicate that the same physics governs the dynamics of Li^+ ions in glasses, particles in colloidal super-cooled liquids and molecules in Lennard-Jones liquids. If this is indeed the case, then a theory of fast relaxation that is applicable to colloidal and molecular super-cooled liquids but *not* to ions in glasses may not be the ultimate explanation that we are looking for.

Recently, Heuer and co-workers [60] also performed MD simulation of lithium metasilicate using similar potentials and, in some ways, their results are comparable to ours.

8. Conflicting points of view

The interpretation given here of the entire conductivity relaxation spectra including the NCL at higher frequencies and its transition at lower frequencies to many-particle ion-hopping conductivity is in conflict with some other points of view. Whilst we emphasize the importance of ion–ion interactions/correlations in determining the many-particle ion hopping, others have proposed very different scenarios. These include the model of Dyre and Schroder [61] and similar models by Hunt [62] and Svare *et al* [63] which all, essentially, describe single particles jumping over random energy barriers in percolative transport. Moynihan and Whang [64] evaluated for a typical sodium trisilicate glass the distribution of conductivity relaxation times caused by structural inhomogeneities and fluctuations in the glass. By contrast with the assumptions of the random energy barrier model, they found that structural inhomogeneities make only a minor contribution to the distribution of conductivity relaxation times. Another approach is reflected in the dynamical structural relaxation model of Bunde, Maass and Ingram [65] for ion transport, which is based on structural rearrangements in the *glassy* state accompanying ion transport. Ion–ion interactions/correlations are not considered to be important in any of these models. Nevertheless, Moynihan and Whang [64] have concluded that ion–ion interactions/correlations are necessary to explain the dispersion of ion transport since structural inhomgeneities cannot.

However, there are models for ion transport that are based on ion–ion interactions/correlations, thus sharing the same physics as our interpretation. The best example is the Coulomb lattice gas model of Maass *et al* [66] which shows that the ac conductivity frequency dependence changes with ion–ion Coulomb interaction strength. Expressed in terms of the electric modulus, this result for the ac conductivity is equivalent to an increase in the width of the electric modulus loss peak with increasing Coulomb interaction. This is just like the interpretation from the CM which has the coupling parameter n in equation (5) increasing with ion–ion interactions, as elucidated by comparing the widths of the electric modulus data for ionic conductors having low ion concentrations (sections 2.4 and 2.5) with those having high ion concentrations (section 2.1–2.3). The Coulomb lattice gas model was further developed and applied to explain the large difference between nuclear magnetic resonance (NMR) and dc conductivity data [67], similar to another explanation provided by the CM [68], and both models are based on ion–ion interactions. Good evidence for the importance of ion–ion interactions/correlations is provided by MD simulations of sodium silicate glasses [24] which show that the product of the sodium diffusion constant and the lifetime of the Na–Na 'bonds' is almost temperature independent. The percolation model provides another explanation of the difference between NMR and conductivity data [63]. Funke's 'concept of mismatch and relaxation' model [69] is a mean-field treatment of the effect that ion–ion interactions have on ionic transport but so far it has not been used to explain the difference between NMR and conductivity data.

This short summary of the different theoretical approaches demonstrates the diversity of ideas in research on the dynamics of ions i.e. a proper approach to the dynamics of ions in glasses, crystals and melts is still a matter of genuine scientific debate. We need to emphasize the experimental facts that can critically falsify a model and not be mesmerized by the few successes of any model used to claim legitimacy by its proponent. An example is the observation that a large number of host alkali ions are immobilized for each foreign alkali ion added in glasses where the concentration of foreign alkali ions is very low [70, 71]. It was shown that ion–ion interactions/correlations could explain this effect [71]. On the other hand, some of the current models for ion conduction in glasses cited above can be immediately ruled out as they do not predict this effect.

Based solely on experimental data plotted as $\log \sigma(\nu)$ versus $\log \nu$, Sidebottom [72, 73] and Roling [73, 74] have claimed that all data can be scaled to a universal master curve, independent of ion concentration, temperature and the chemical structure of a glass or melt. The claim that all ionic conductors, with widely different chemical and physical structures and greatly varying ion concentrations, all have the same dispersion is amazing. In spite of this spectacular claim, no credible theoretical support has been offered. For example, it has been shown by several groups [17, 18], including the proponent of universal scaling [75], that the shapes of $\log \sigma(\nu)$ versus $\log \nu$ plots depend on the composition and ion concentration of the glass and that the conductivity spectra of glasses cannot be scaled to a universal function as claimed. These breakdowns are rationalized by making various assumptions like the dimensionality of transport and the participation of other kinds of ion. Nevertheless, universal scaling of the real part of the conductivity is still very much the belief of its proponents.

The stumbling block to universal scaling is that the *same* data in the electric modulus representation do not scale. A way out of this dilemma for advocates of universal scaling is to find fault with the electric modulus representation of data. They fault the electric modulus because the high-frequency dielectric constant, ε_∞, enters explicitly into its definition by equation (4) but has nothing to do with the ion dynamics. With this 'fault', they jump to the conclusion that data in the electric modulus representation do not reflect the true dynamics of the ions. However, this is *not* a fault of the electric modulus because it has been shown [76] that

the approximate time dependence of the Fourier transform of the electric modulus given by equation (5) accounts not only for the frequency dependence of the real and imaginary parts of the electric modulus M^* but also for the magnitude of the dielectric strength for ionic motion, $\Delta\varepsilon = \varepsilon_s - \varepsilon_\infty$, where ε_s is the low-frequency compliance contributed from the mobile ions. Moreover, M^* can now be *directly* measured by new instrumentation introduced by Richert and Wagner [77]. On the other hand, the proponents of universal scaling for the real part of $\sigma^*(\nu)$ never show the imaginary part of $\sigma^*(\nu)$, whether it scales, or how ε_∞ enters into it.

In mechanical spectroscopy, the exact analogues of $M^*(\omega)$, $\varepsilon^*(\omega)$ and $\sigma^*(\omega)$ are the complex dynamic modulus $G^*(\omega)$, the complex dynamic compliance $J^*(\omega)$ and the reciprocal of the complex dynamic viscosity $1/\eta^*(\omega)$ for a (flowing) viscoelastic liquid respectively [78]. The electric modulus representation relates the dc conductivity to the mean electric modulus relaxation time through $\sigma = \varepsilon_\infty/\langle\tau\rangle$. This relation, often criticized by the proponents of universal scaling, has an exact analogue in the well known Maxwell relation, $1/\eta = (G_\infty)^{-1}/\langle\tau\rangle$, between the fluidity, $1/\eta$, the mean mechanical relaxation time and the high-frequency modulus G_∞. Various makes of instrument available in most laboratories for mechanical studies directly measure either $G^*(\omega)$ or the relaxation modulus $G(t)$. The two are related by the Fourier transforms

$$G'(\omega) = \omega \int_0^\infty G(t) \sin \omega t \, \mathrm{d}t, \tag{15}$$

$$G''(\omega) = \omega \int_0^\infty G(t) \cos \omega t \, \mathrm{d}t, \tag{16}$$

which can be found in textbooks such as [78] (see equations (39) and (40) therein). $G(t)$ is often rewritten as the product $G_\infty\Phi(t)$ and $\Phi(t)$ decays monotonically from one to zero, like the Kohlrausch function of equation (5). After partial integration, equations (15) and (16) have the combined form

$$G^*(\omega) = G'(\omega) + \mathrm{i}G''(\omega) = G_\infty\left[1 - \int_0^\infty \mathrm{d}t \, \mathrm{e}^{-\mathrm{i}\omega t}(-\mathrm{d}\Phi/\mathrm{d}t)\right], \tag{17}$$

which is the exact analogue of equation (4) for the electric modulus. The criticism that ε_∞ enters explicitly into the electric modulus applies verbatim to equation (17), where G_∞ replaces ε_∞, and hence also to equations (15) and (16). Thus the critics of the electric modulus, in saying that it does not reflect the dynamics of the ions, have no choice but to dispute the use and measurement of the dynamic complex modulus of viscoelastic liquids [78] and they also have to say that it does not correctly give the dispersion of the molecular motions. This challenge would be ill advised because the community of workers in mechanical relaxation, with their voluminous amount of published literature, shows no sign of any doubt that macroscopic measurements of the complex dynamic modulus truly reflect the dynamics and frequency dispersion of the molecular motions [78].

9. Conclusion

From a combined study of the ion dynamics by an analysis of experimental data, use of the CM predictions and MD simulations we have an improved understanding of the ion dynamics in the three principal time/frequency regimes: the NCL at high frequencies, a transition zone at intermediate frequencies and the many-particle ion-hopping regime at low frequencies. The NCL corresponds to a very slow rise with respect to time of the MSD of the Li^+ ions, $\langle r^2\rangle$, and to a very slow cage decay time, properties that are shown to be synergistic in the short-time regime where the majority of the ions can be considered to be confined. Ultimately the

cause of the cage decay is thermally activated independent (i.e. free from other ion influence) jumps of the Li^+ ions from their original sites. At sufficiently low temperature and short times, such free jumps are few but nevertheless the probability increases slowly with time. Thus the cages decay very slowly as long as the time is much shorter than the independent free jump relaxation time, $\tau_0(T)$. The latter, for several glassy ionic conductors, has been deduced from experimental data by application of the CM. Indeed we find that the NCL exists only at times $t < t_{x1}$ and that t_{x1} is much shorter than $\tau_0(T)$. This description is supported by the time dependence of the self-part of the van Hove correlation function, $G_s(r, t)$, for the Li^+ ions in Li_2SiO_3. In fact we find from $4\pi r^2 G_s(r, t)$ in the short-time regime $t < t_{x1}$ that free jumps to neighbouring sites are few and increase very slowly with time.

Experimental data indicate that a description of the dielectric relaxation data by equation (4) using the stretched exponential decay function of equation (5) (the many-particle ion-hopping regime) is valid only at times longer than t_{x2}. Thus the intermediate-time regime, $t_{x1} < t < t_{x2}$, is the transition zone from the NCL to the many-particle ion-hopping regime. We find invariably that $\tau_0 < t_{x2}$, leading naturally to the understanding that many-particle ion hopping can commence only when all ions have a high probability of attempting an independent hop. From MD simulations, the change of $4\pi r^2 G_s(r, t)$ with time is found to be more rapid in the transition zone, $t_{x1} < t < t_{x2}$, than in the NCL regime, indicating a more rapid cage decay. A more rapid increase of $\langle r^2 \rangle$ with time is found in this regime but its time dependence does not become a power law until after t_{x2} The width of the crossover region seems a bit larger in glasses having a smaller exponent, $1 - n$, of the stretched exponential decay function for the many-particle ion hopping given by equation (5).

As discussed above, after t_{x2} the dielectric data are well described by equations (4) and (5), indicating the establishment of a many-particle ion-hopping regime. The loss modulus, $M''(\nu)$, has a power law dependence ν^{n-1} for $(2\pi\nu\tau_K) \gg 1$ and ν^1 for $(2\pi\nu\tau_K) \ll 1$. The former corresponds to a ν^n dependence of the conductivity and the latter to the dc conductivity, both of which are consequences of the Maxwell relation. MD simulations indicate that in the penultimate time regime, $t_{x2} < t < \tau_K$, the MSD, $\langle r^2 \rangle$, has primarily a power law time dependence t^{1-n}. Finally for $t \gg \tau_K$, the MSD is proportional to t. In the time regime $t_{x2} < t < \tau_K$, a second peak at a distance between Li^+ ion sites develops in $4\pi r^2 G_s(r, t)$ and grows with time, indicating that a significant number of Li^+ ions have jumped from their cages to neighbouring sites to participate in co-operative motion at longer distances. The self-part of the Li^+ ion density correlation function, $F_s(k, t)$, in the same time regime is a stretched exponential function of time, which is a signature of co-operative or collective dynamics. The stretch exponent of $F_s(k, t)$ for $k = 2\pi/3$ Å^{-1} is nearly the same as the exponent, $(1 - n)$, in the time dependence of $\langle r^2 \rangle \propto t^{1-n}$. We have used the normalized area of the first and second peaks of $4\pi r^2 G_s(r, t)$ to gauge the progress of cage decay, and find that its time dependence is similar to that of $\langle r^2 \rangle$ in all three time regimes. Thus the MSD and cage decay are synergistic properties.

Although the present work is focused on ionic glasses, fittingly we have also brought into discussion the experimental data for colloidal super-cooled liquids. The similarity in the dynamics of the two systems is remarkable. In colloidal super-cooled liquids with high volume fractions, over an extensive short-time regime the MSD of the colloidal particles increases very slowly with the logarithm of time ($\langle r^2 \rangle \propto t^{0.08}$). Crossover times, t_{x1} and t_{x2}, with the same physical meanings as for Li_2SiO_3, and a separation of the dynamics into several time regimes, are also found in colloidal systems. In the latter, Weeks and Weitz obtained from experiment a cage decay correlation function and its time dependence is found to be similar to that of the first and second peaks of the self-part of the Li^+ ion van Hove correlation function. In particular, both systems show very slow cage decay in the regime $t < t_{x1}$, slow decay in the

regime $t_{x1} < t < t_{x2}$ and faster decay in the regime $t > t_{x2}$. In both systems the non-Gaussian parameter $\alpha_2(t)$ is a broad peak with a maximum at approximately t_{x2}. The dynamics of both systems show the presence of fast- and slow-moving colloidal particles or Li^+ ions. The distinction between fast- and slow-moving particles becomes increasingly clear at times after t_{x2}. The striking similarities of the two systems may or may not be due to the fact that the colloidal systems studied by Weeks and Weitz are slightly charged. In spite of the similarities, an ionic glass and a super-cooled colloidal liquid have differences. One is the presence of much more immobile matrix atoms along side mobile ions in the glass. We have not discussed the MD simulation results for Lennard-Jones liquids in any detail. Nevertheless, for some of the properties discussed, a Lennard-Jones super-cooled liquid behaves like the Li_2SiO_3 glass and the colloidal super-cooled liquid. It is likely that all three systems share the same basic physics governing the relaxation and diffusion of interacting particles. Therefore a theory proposed to explain the dynamics in any one of these systems is viable only if it is applicable to the other two.

Acknowledgments

Some of the calculations in this work were performed with an SX-3/34R and SX-5 computer at the Research Center for Computational Science. The CPU time made available is gratefully acknowledged. The work performed at the Naval Research Laboratory was supported by the Office of Naval Research. We thank Peter Lunkenheimer, H Jain, Ajit Kulkarni and Annie Pradel for making their experimental data available to us.

References

[1] Garton G C 1946 *Discuss. Faraday Soc.* A **42** 161
[2] Owen A E 1963 *Prog. Ceram. Sci.* **3** 77
[3] Stevels J M 1957 *Handbuch Phys.* **20** 372
[4] Wong J and Angell C A 1976 *Glass Structure by Spectroscopy* (New York: Dekker)
[5] Ngai K L, Rendell R W and Jain H 1984 *Phys. Rev.* B **30** 2133
[6] Burns A, Chryssikos G D, Tombari E, Cole R H and Risen W M 1989 *Phys. Chem. Glasses* **30** 264
[7] Lee W K, Liu J F and Nowick A S 1991 *Phys. Rev. Lett.* **67** 1559
[8] Lu X and Jain H 1994 *J. Phys. Chem. Solids* **55** 1433
[9] Jain H and Lu X 1996 *J. Non-Cryst. Solids* **196** 285
[10] León C, Lucia M L and Santamaria J 1997 *Phys. Rev.* B **55** 882
[11] Ngai K L, Jain H and Kanert O 1997 *J. Non-Cryst. Solids* **222** 383
[12] Nowick A S, Vaysleb A V and Liu W 1998 *Solid State Ion.* **105** 121
[13] Belin R, Taillades G, Pradel A and Ribes M 2000 *Solid State Ion.* **136/137** 1025
[14] Funke K, Heimann B, Vering M and Wilmer D 2001 *J. Electrochem. Soc.* A **148** 395
[15] Patel H and Martin S W 1992 *Phys. Rev.* B **45** 10292
[16] Ngai K L 1999 *J. Chem. Phys.* **110** 10576
[17] Ngai K L and Moynihan C T 1998 *Bull. Mater. Res. Soc.* **23** 51
[18] Jain H and Krishnaswami S 1998 *Solid State Ion.* **105** 129
[19] Nowick A S, Lim B S and Vaysleb A V 1994 *J. Non-Cryst. Solids* **172–174** 1243
[20] León C, Rivera A, Várez A, Sanz J, Santamaría J and Ngai K L 2001 *Phys. Rev. Lett.* **86** 1279
[21] Rivera A, León C, Varsamis C P E, Chryssikos G D, Ngai K L, Roland C M and Buckley L J 2002 *Phys. Rev. Lett.* **88** 125902
[22] Jonscher A K 1983 *Dielectric Relaxation in Solids* (London: Chelsea)
[23] For a review of various representations of conductivity relaxation data see
Moynihan C T 1994 *J. Non-Cryst. Solids* **172–174** 1395
Moynihan C T 1996 *J. Non-Cryst. Solids* **203** 359
Moynihan C T 1998 *Solid State Ion.* **105** 75
[24] Binder K 2000 *J. Non-Cryst. Solids* **274** 332

[25] Strom U, Ngai K L and Kanert O 1991 *J. Non-Cryst. Solids* **131–133** 1011
[26] León C, Santamaria J, Paris M A, Sanz J, Ibarra J and Torres L M 1997 *Phys. Rev.* B **56** 5302
[27] León C, Lucia M L, Santamaria J and Sánchez-Quesada F 1998 *Phys. Rev.* B **57** 41
[28] Ngai K L 1979 *Comments Solid State Phys.* **9** 121
[29] Tsang K Y and Ngai K L 1997 *Phys. Rev.* E **56** R17
[30] Ngai K L 1998 *Phil. Mag.* **77** 187
[31] Ngai K L, Greaves G N and Moynihan C T 1998 *Phys. Rev. Lett.* **80** 1018
[32] Greaves G N and Ngai K L 1995 *Phys. Rev.* B **52** 6358
[33] Lunkenheimer P, Pimenov A and Loidl A 1997 *Phys. Rev. Lett.* **78** 2995
[34] Lunkenheimer P 1999 *Dielectric Spectroscopy of Glassy Dynamics* (Aachen: Shaker)
[35] Kulkarni A, Lunkenheimer P and Loidl A 1999 *Ceram. Trans.* **92** 115
[36] Ribes M, Bychkov E and Pradel A 2001 *J. Optoelectron. Adv. Mater.* **3** 665
[37] Simmons J H, Elterman P B, Simmons C J and Mohr R K 1979 *J. Am. Ceram. Soc.* **62** 158
[38] Cramer C, Funke K and Saatkamp T 1995 *Phil. Mag.* **71** 701
[39] Ngai K L, Cramer C, Saatkamp T and Funke K 1996 *Non-Equilibrium Phenomena in Supercooled Fluids, Glasses and Amorphous Materials* ed M Giordano, D Leporini and M P Tosi (Singapore: World Scientific) p 3
[40] Ngai K L 1992 *J. Physique Coll.* **2** C2 61
[41] Ngai K L and Kanert O 1992 *Solid State Ion.* **53–55** 936
[42] Funke K 1993 *Prog. Solid State Chem.* **22** 111
[43] Cramer C and Buscher M 1998 *Solid State Ion.* **105** 109
[44] Ngai K L 1999 *J. Non-Cryst. Solids* **248** 194
[45] Ngai K L and Strom U 1988 *Phys. Rev.* B **38** 10350
[46] Tachez M, Mercier R, Malugani J P and Dianoux A J 1986 *Solid State Ion.* **20** 93
[47] Dianoux A J, Tachez M, Mercier R and Malugani J P 1991 *J. Non-Cryst. Solids* **131–133** 973
[48] Owens A P, Pradel A, Ribes M and Elliott S R 1991 *J. Non-Cryst. Solids* **131–133** 1104
Owens A P, Pradel A, Ribes M and Elliott S R 1991 *Mater. Res. Soc. Symp. Proc.* **210** 621
[49] Kubo R 1957 *J. Phys. Soc. Japan* **12** 570
[50] Gilroy K S and Phillips W A 1981 *Phil. Mag.* B **43** 735
[51] Habasaki J, Okada I and Hiwatari Y 1995 *J. Non-Cryst. Solids* **183** 12
Habasaki J, Okada I and Hiwatari Y 1995 *Phys. Rev.* E **52** 2681
Habasaki J, Okada I and Hiwatari Y 1997 *Phys. Rev.* B **55** 6309
Habasaki J, Okada I and Hiwatari Y 1998 *J. Phys. Soc. Japan* **67** 2012
[52] Habasaki J and Hiwatari Y 1998 *Phys. Rev.* E **58** 5111
Habasaki J and Hiwatari Y 1999 *Phys. Rev.* E **59** 6962
[53] Habasaki J, Ngai K L and Hiwatari Y 2002 *Phys. Rev.* E **66** 021205
[54] Ida Y 1976 *Phys. Earth Planet. Inter.* **13** 97
[55] Habasaki J and Okada I 1992 *Mol. Simul.* **9** 319
[56] Weeks E R and Weitz D A 2002 *Phys. Rev. Lett.* **89** 095704
[57] Rahman A 1964 *Phys. Rev.* A **136** 405
[58] Weeks E R, Crocker J C, Levitt A, Schofield A and Weitz D A 2000 *Science* **287** 627
[59] Kob W, Donati C, Plimton S J, Poole P H and Glotzer S C 1997 *Phys. Rev. Lett.* **79** 2827
[60] Heuer A, Kunow M, Vogel M and Banhatti R D 2002 *Phys. Chem. Chem. Phys.* **4** 3185
[61] Dyre J and Schroder T B 2000 *Rev. Mod. Phys.* **72** 873
[62] Hunt A G 2001 *Phil. Mag.* B **81** 875
[63] Svare I, Borsa F, Torgeson D R and Martin S W 1994 *J. Non-Cryst. Solids* **172–174** 1300
[64] Moynihan C T and Whang J-H 1997 *Mat. Res. Soc. Symp. Proc.* vol 455 (Warrendale, PA: Materials Research Society) p 133
[65] Maass P, Bunde A and Ingram M D 1992 *Phys. Rev. Lett.* **68** 3064
[66] Maass P, Petersen J, Bunde A, Dieterich W and Roman H E 1991 *Phys. Rev. Lett.* **66** 52
[67] Maass P, Meyer A, Bunde A and Dieterich W 1996 *Phys. Rev. Lett.* **77** 1528
[68] Ngai K L 1993 *J. Chem. Phys.* **98** 6424
Ngai K L 1993 *Phys. Rev.* B **48** 13481
[69] Funke K, Banhatti R D, Brueckner S, Cramer C, Krieger C, Mandanici A, Martiny C and Ross I 2002 *Phys. Chem. Chem. Phys.* **4** 3155
[70] Moynihan C T, Saad N S, Tran D C and Lesikar A V 1980 *J. Am. Ceram. Soc.* **63** 458
[71] Ngai K L, Wang Y and Moynihan C T 2002 *J. Non-Cryst. Solids* **307–310** 999
[72] Sidebottom D L 1999 *Phys. Rev. Lett.* **82** 3653

[73] Sidebottom D L, Roling B and Funke K 2001 *Phys. Rev.* B **63** 024310
[74] Roling B, Martiny C and Murugavel S 2001 *Phys. Rev. Lett.* **87** 085901
See comment by
León C, Rivera A, Santamaría J, Moynihan C T and Ngai K L 2002 *Phys. Rev. Lett.* **80** 079601
[75] Roling B and Martiny C 2000 *Phys. Rev. Lett.* **85** 1274
[76] Ngai K L and Rendell R W 2000 *Phys. Rev.* B **61** 9397
[77] Richert R and Wagner H 1998 *Solid State Ion.* **105** 167
[78] Ferry J D 1980 *Viscoelastic Properties of Polymers* 3rd edn (New York: Wiley)